Journal of Computational Physics **180,** 597–615 (2002)
doi:10.1006/jcph.2002.7108

Accurate ω-ψ Spectral Solution of the Singular Driven Cavity Problem

F. Auteri, L. Quartapelle, and L. Vigevano

Dipartimento di Ingegneria Aerospaziale, Politecnico di Milano, Via La Masa 34, 20158 Milan, Italy
E-mail: auteri@aero.polimi.it

Received June 25, 2001; revised March 5, 2002

This article provides accurate spectral solutions of the driven cavity problem, calculated in the vorticity–stream function representation without smoothing the corner singularities—a *prima facie* impossible task. As in a recent benchmark spectral calculation by primitive variables of Botella and Peyret, closed-form contributions of the singular solution for both zero and finite Reynolds numbers are subtracted from the unknown of the problem tackled here numerically in biharmonic form. The method employed is based on a split approach to the vorticity and stream function equations, a Galerkin–Legendre approximation of the problem for the perturbation, and an evaluation of the nonlinear terms by Gauss–Legendre numerical integration. Results computed for $\mathrm{Re} = 0$, 100, and 1000 compare well with the benchmark steady solutions provided by the aforementioned collocation–Chebyshev projection method. The validity of the proposed singularity subtraction scheme for computing time-dependent solutions is also established.

Key Words: driven cavity problem; corner singularity; vorticity and stream function formulation; Navier–Stokes equations; Galerkin–Legendre spectral methods; Glowinski–Pironneau method.

1. INTRODUCTION

In a recent paper, Botella and Peyret provided benchmark results for the steady problem in a square cavity using a pseudospectral Chebyshev approximation to solve the Navier–Stokes equations by means of a fractional-step projection method [5]. The boundary conditions considered in that work are exactly as in the earlier FD computations by Burggraf [6]. This means that the solution has a singular behavior at the two upper corners, where the horizontal wall slides on the fixed vertical walls of the cavity. To avoid the Gibbs' phenomenon induced by the singularities and to improve the accuracy, the unknown variables of the problem where changed by subtracting solution components associated with the corner singularities, as provided by the analysis of Batchelor [3] and its extension of Gupta, Manohar and Noble [9].

0021-9991/02 $35.00

The aim of the present paper is to show that results of a comparable accuracy to that of the spectral projection method can be achieved also using the vorticity–stream function formulation of the 2D Navier–Stokes equations and a suitable spectral method.

Accounting for the singular component of the solution to the incompressible Navier–Stokes equations can be troublesome in some discrete form of the singular problem since the pressure and the vorticity diverge at the two corners, where the leading term of the singular solution behaves as $1/r$, r being the distance from the corner. As a consequence, any spectral method which samples the pressure or vorticity field at the two singular corners, as collocation schemes using Gauss–Lobatto points typically do, is unable to solve the driven cavity problem unless the singularity is eliminated by a suitable *regularization* of the velocity boundary conditions, thus leading to an essentially different problem.

In this respect, a somewhat different difficulty, but still related to the use of collocation points, was faced by Schultz, Lee, and Boyd [18], where the first application of the corner singularity subtraction technique in a spectral context was proposed. In this case, the tau–Chebyshev method was used to solve the fourth-order biharmonic equation in a cavity. The authors reported that the set of algebraic equations so obtained was either an undetermined system or a slightly overdetermined system. To overcome the indeterminacy, a least-squares approach was adopted.

The difficulties met by collocation schemes are not faced by the fractional-step method based on a Poisson equation for pressure considered by Botella and Peyret [5]. In fact, in the projection method the solution singularity occurs in the pressure field which is governed by a Neumann boundary value problem, while the velocity field, solution to a Dirichlet problem, is finite in the corners. Stated in other words, in the projection method the boundary value of the pressure does not enter the spectral solution algorithm: the collocation points of the Neumann problem for pressure are all internal to the domain, while the Gauss–Lobatto points located on the boundary are used to enforce the Dirichlet conditions for the velocity, and do not involve the pressure variable. For these reasons Botella and Peyret succeeded in solving the driven cavity problem by subtracting the singular component of the solution within a spectral-collocation projection method and obtained steady solutions not contaminated by Gibbs' spatial oscillations.

In the present paper we show that the same convergence can also be achieved using a vorticity and stream function formulation by applying the uncoupled spectral solver recently proposed by the first two authors [1]. The method is based on a Galerkin–Legendre weak formulation of the linear equations for the nonprimitive variables, operating only on the Legendre coefficients of the unknowns, and employs standard Gauss–Legendre numerical integration to evaluate the nonlinear terms. As a consequence, the singular component of the vorticity is sampled only in the interior of the computational domain while, at the same time, the trace of the vorticity, with its corner values included, is accommodated within the solution algorithm, since the vorticity perturbation unknown is a regular function which assumes finite values on the entire boundary.

2. THE SINGULAR ω-ψ DRIVEN CAVITY PROBLEM

In this section we first define the driven cavity problem in the vorticity and stream function representation. In Section 2.1 we specify the boundary conditions on the four walls of the square domain for the singular (not regularized) problem and give a complete discussion of the compatibility conditions on the boundary data of the biharmonic problem in a square

domain. In Section 2.2 we recall the expansion of the corner singular solution, including the first two terms of the series provided by Gupta *et al*. [9] and also considered by Botella and Peyret [5]. The focus here is only on the mathematical aspects of the corner singularity; for a discussion on the limits of the continuum model to represent the physical processes in the singular region from a molecular dynamics viewpoint the reader is referred to [13]. Finally, in Section 2.3, we describe the behavior of the two components of the singular solution.

2.1. Singularity and Compatibility Conditions

The Navier–Stokes equations for unsteady 2D flows expressed in terms of the variables vorticity ω and stream function ψ read

$$\frac{\partial \omega}{\partial t} + J(\omega, \psi) = \frac{1}{\mathrm{Re}} \nabla^2 \omega \quad \text{and} \quad -\nabla^2 \psi = \omega, \tag{2.1}$$

where J denotes the Jacobian determinant with respect to the x–y coordinates and Re is the Reynolds number. We consider a unit square domain $\Omega = (0, 1)^2$ with the top wall sliding toward the left at a unit velocity. The top, bottom, left, and right sides are denoted, respectively, Γ_t, Γ_b, Γ_l, and Γ_r, as shown in Fig. 1. The boundary conditions for ψ are therefore given by

$$\psi_{|\Gamma} = 0 \quad \text{and} \quad \begin{cases} \frac{\partial \psi}{\partial n}_{|\Gamma_t} = 1, \\ \frac{\partial \psi}{\partial n}_{|\Gamma \setminus \Gamma_t} = 0. \end{cases} \tag{2.2}$$

According to the theoretical analysis of Bernardi and Maday [4], the well-posedness of the boundary value problem for the biharmonic operator in a rectangular domain requires that the boundary data satisfy *three sets* of compatibility conditions at the four corners:

1. Compatibility conditions involving only the values of the Dirichlet datum.
2. Compatibility conditions between the Dirichlet and the Neumann data.
3. Compatibility conditions pertaining only to the Neumann datum.

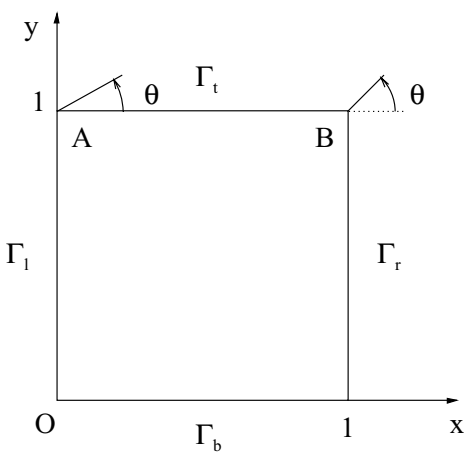

FIG. 1. Geometry of the driven cavity problem, with its side denotation and the singular corners.

The compatibility conditions of the first set are simply that the Dirichlet profiles on the four sides must be *continuous* at the four corners [4, p. 167]: these conditions are trivially satisfied in the driven cavity problem considered above. Notice that the continuity of the Dirichlet datum at the corners is a compatibility condition also for the elliptic equation involving the Laplace operator (cf. [4, p. 93]).

The second set of compatibility conditions for the well-posedness of the biharmonic problem requires that at each corner the tangential derivative of the Dirichlet profile on one side be coincident with the corner value of the Neumann profile on the other, concurrent side ([4], p. 169). In the boundary conditions of driven cavity problem above, two conditions among the total of eight such compatibility conditions are not satisfied at the *two upper corners*. This is the theoretical reason for the need of a proper treatment of the corner singularities in the numerical solution of the singular driven cavity problem.

Finally, the last set of compatibility conditions for the biharmonic problem requires that the tangential derivatives of the two Neumann profiles be equal at each corner (up to the sign) [4, p. 169, Eq. (2.17)]. These four compatibility conditions are associated with the equality of the mixed second derivatives of the unknown at the corners and are satisfied by the Neumann datum of the driven cavity problem.

We notice that Barragy and Carey [2] modified the original Neumann condition for ψ on the upper sliding wall by replacing the uniform profile with a trapezoidal profile vanishing at the singular corners. In this way, all eight compatibility conditions between the Dirichlet and Neumann data are respected but the third set of compatibility conditions on the Neumann datum is violated at the singular corners. As a matter of fact, since the compatibility conditions of the third set are in some sense weaker than those between the Dirichlet and Neumann data, their violation does not prevent to obtain accurate results of the steady ω-ψ equations at high Reynolds numbers by means of the p-method on nonuniform meshes [2]. In any case, the problem solved by these authors approaches the unregularized driven cavity problem considered in the present work only asymptotically, as the mesh is infinitely refined.

It must be emphasized that the violation of the compatibility conditions of the second set occurring in the singular driven cavity problem does not prevent its numerical solution by a properly constructed spectral approximation. For instance, a Galerkin spectral method for the vorticity and stream function equations relying on Gauss–Legendre quadrature points (as opposed to the Gauss–Lobatto ones) has been developed by the present authors [1]. This scheme has provided correct numerical solutions to the singular driven cavity problem, without regularization, but for the occurrence of the expected phenomenon of Gibbs' oscillations. The spatial oscillations are triggered by the presence of the corner singularity. The purpose of the present work is to show that the subtraction of the singular components completely eliminates Gibbs' spatial oscillations from the Galerkin–Legendre spectral solution to the vorticity and stream function equations.

2.2. Singular Solution in the Corners

Following the analysis of creeping flow by Batchelor [3], the behavior of the flow in a corner with one sliding wall and one fixed wall can be determined analytically as an asymptotic expansion of the solution in the proximity of the corner.

A general expression of the singularity for creeping flows is provided by the well-known theory of Moffatt, which gives a separated series expansion of powers of the distance

from the corner with complex exponent. The first few terms of this expansion have been taken into account by Ingham and Kelmanson in solving the biharmonic problem for the driven cavity by means of a modified boundary integral method [12] (see also [11, Chap. 3]).

When the effects of inertia are no longer negligible, further terms have to be taken into account. In this respect, Gupta *et al*. determined the solution as an expansion in powers of the Reynolds number [9], neglecting the contribution due to the eigenfunctions of the Stokes operator for homogeneous boundary conditions. A more general solution was provided by Hancock *et al*., who took into account these additional terms [10]. In the present work, only the two leading terms of the expansion of the solution to the fourth-order equation are retained, exactly as in [5], the role of higher order terms being left for further investigations.

Let A and B denote, respectively, the left and right upper corners of the square cavity (see Fig. 1). We consider first the singularity of the solution in corner A by introducing a polar coordinate system (r, θ) centered in the corner, so that the fluid is in the region with $-\pi/2 \le \theta \le 0$. The first two terms of the expansion for the vorticity are written in the form

$$\omega^A(r, \theta; \mathrm{Re}) = \omega_0^A(r, \theta) + \mathrm{Re}\, \omega_1^A(r, \theta), \tag{2.3}$$

and similarly for the stream function. The boundary conditions accounting for the motion of the horizontal wall and the rest of the vertical wall are, for the singularity in the left corner,

$$\begin{cases} \psi^A = 0, & \frac{\partial \psi^A}{\partial n} = 1, \quad \text{for } \theta = 0, \\ \psi^A = 0, & \frac{\partial \psi^A}{\partial n} = 0, \quad \text{for } \theta = -\frac{\pi}{2}. \end{cases} \tag{2.4}$$

The Stokes contribution to the singular solution is obtained considering the biharmonic problem consisting in the two equations

$$\nabla^2 \omega_0^A = 0 \quad \text{and} \quad \nabla^2 \psi_0^A = -\omega_0^A, \tag{2.5}$$

to be solved in the domain $r > 0$ and $-\pi/2 < \theta < 0$, under the boundary conditions $\psi_0^A = 0$, $(\partial \psi_0^A / \partial n) = 1$ for $\theta = 0$ and $\psi_0^A = 0$, $(\partial \psi_0^A / \partial n) = 0$ for $\theta = -\pi/2$.

Then, the first-order-in-Re contribution is obtained by solving the system of two equations,

$$\nabla^2 \omega_1^A = J\left(\omega_0^A, \psi_0^A\right) \quad \text{and} \quad \nabla^2 \psi_1^A = -\omega_1^A, \tag{2.6}$$

supplemented by fully homogeneous boundary conditions, namely, $\psi_1^A = 0$ and $(\partial \psi_1^A / \partial n) = 0$ for both $\theta = 0$ and $\theta = -\pi/2$ (for details see Gupta, Manohar, and Noble [9]). The boundary conditions imposed on the singular component(s) account for the incompatibility in the data of the boundary conditions (2.2) of the singular driven cavity problem and, at the same time, do not introduce the violation of any other compatibility conditions, as it can be easily checked. For conciseness, we do not report the expressions for ω^A and ψ^A, which can be found, e.g., in [5].

2.3. Components of the Singular Solution

As anticipated, the steady solution of the corner singularity considered in the present work comprises two analytical components: the first one associated with the Stokes problem and the second one proportional to the Reynolds number, associated with the solution of the same Stokes operator but with a given source term. The expressions of the vorticity field and the stream function of the singular solution are

$$\begin{cases} \omega^{A+B}(r, \theta; \mathrm{Re}) = \omega_0^{A+B}(r, \theta) + \mathrm{Re}\ \omega_1^{A+B}(r, \theta), \\ \psi^{A+B}(r, \theta; \mathrm{Re}) = \psi_0^{A+B}(r, \theta) + \mathrm{Re}\ \psi_1^{A+B}(r, \theta). \end{cases}$$

To clarify the effect of including either only the Stokes component or both components, we show in Figs. 2 and 3 the plots of the vorticity fields and the streamlines, respectively. In each figure the behavior of the two separate contributions as well as their sum for the representative value of Reynolds number $\mathrm{Re} = 100$ are displayed, for comparison. As

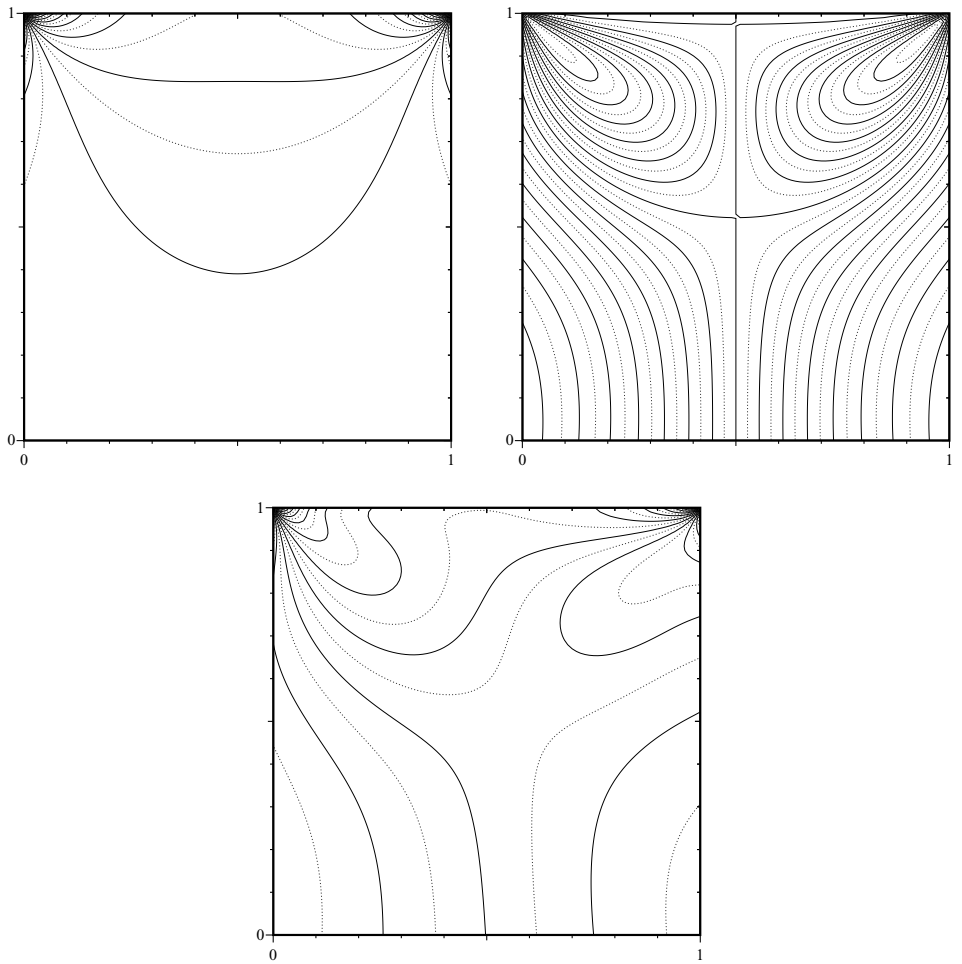

FIG. 2. Vorticity levels of the singular components of the driven cavity problem. (Top left) Zeroth-order contribution ω_0^{A+B}; (top right) first-order-in-Re contribution ω_1^{A+B}; (bottom) superposition of the contributions $\omega_0^{A+B} + \mathrm{Re}\,\omega_1^{A+B}$ for $\mathrm{Re} = 100$.

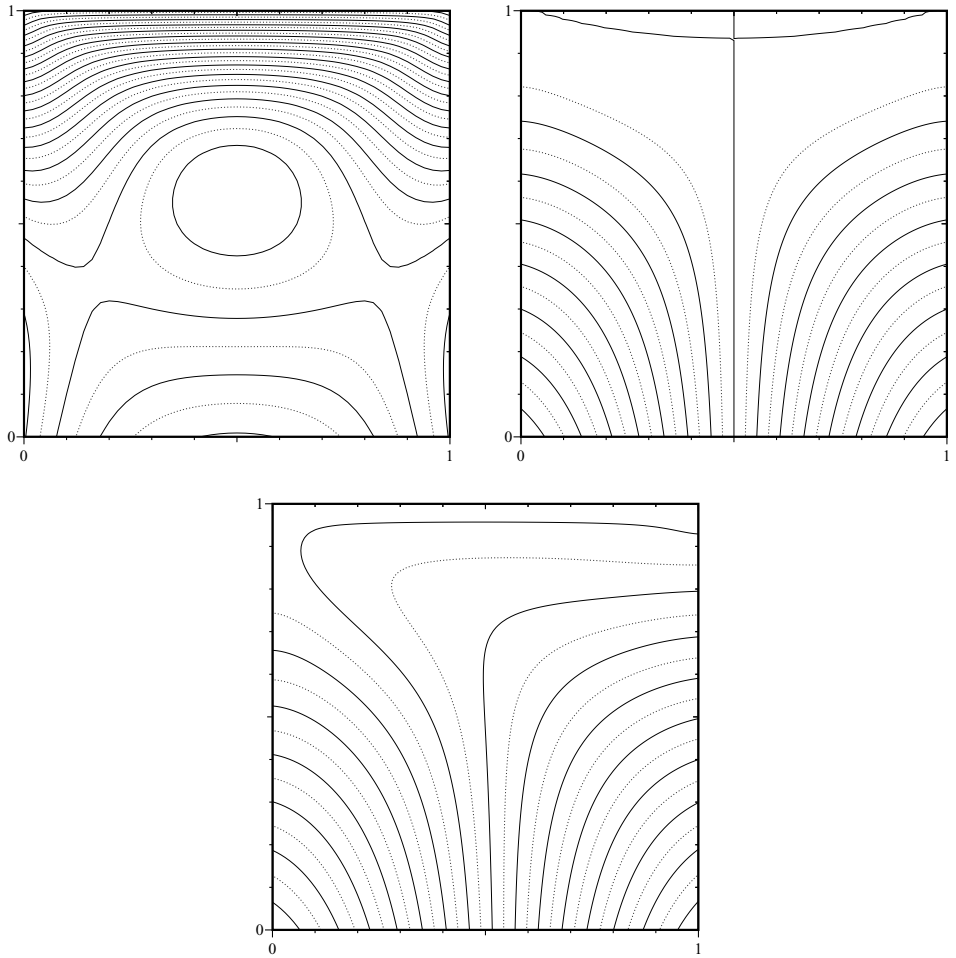

FIG. 3. Streamlines of the singular components of the driven cavity problem. (Top left) Zeroth-order contribution ψ_0^{A+B}; (top right) first-order-in-Re contribution ψ_1^{A+B}; (bottom) superposition of the contributions $\psi_0^{A+B} + \mathrm{Re}\,\psi_1^{A+B}$ for $\mathrm{Re} = 100$.

expected, the singularity of the Stokes component is much stronger than that associated with the first-order-in-Re component. The latter breaks the symmetry with respect to the midline $x = \frac{1}{2}$.

3. THE ω'-ψ' PERTURBATION PROBLEM

We now formulate the problem with the singularities subtracted by specifying the equations governing the perturbation unknowns ω' and ψ' defined by the relations

$$\begin{cases} \omega(\boldsymbol{x}, t) = \omega'(\boldsymbol{x}, t) + \omega^{A+B}(\boldsymbol{x}) = \omega'(\boldsymbol{x}, t) + \omega^{A}(\boldsymbol{x}) + \omega^{B}(\boldsymbol{x}), \\ \psi(\boldsymbol{x}, t) = \psi'(\boldsymbol{x}, t) + \psi^{A+B}(\boldsymbol{x}) = \psi'(\boldsymbol{x}, t) + \psi^{A}(x) + \psi^{B}(x). \end{cases} \tag{3.1}$$

The precise form of the perturbed problem is stated in Section 3.1 and the boundary conditions for ψ' are derived in Section 3.2. Then, we describe the algorithm for the time

discretization of the equations governing the variables ω' and ψ' in Section 3.3. Finally, we outline the Galerkin–Legendre spectral method employed for the spatial approximation in Section 3.4.

3.1. Governing Equations

Substituting (3.1) into the ω-ψ equations (2.1) gives for the following system for the perturbation unknowns ω' and ψ':

$$\begin{cases} \mathrm{Re}\dfrac{\partial \omega'}{\partial t} + \mathrm{Re}J(\omega' + \omega^{A+B}, \psi' + \psi^{A+B}) = \nabla^2(\omega' + \omega^{A+B}), \\ -\nabla^2\psi' = \omega'. \end{cases} \tag{3.2}$$

We note that no singular solution component appears in the Poisson equation since the fields ψ^A and ω^A are such that $-\nabla^2\psi^A = \omega^A$ identically, and similarly for ψ^B and ω^B. Eventually, we can write the vorticity equation in the form

$$\mathrm{Re}\frac{\partial \omega'}{\partial t} - \nabla^2\omega' = \nabla^2\omega^{A+B} - \mathrm{Re}J(\omega' + \omega^{A+B}, \psi' + \psi^{A+B}), \tag{3.3}$$

where we retain on the left hand side only the terms to be treated implicitly in the time-stepping algorithm that will be introduced below.

3.2. Boundary Conditions

The stream function ψ' must satisfy boundary conditions which are derived from the boundary conditions (2.2) originally attached to ψ and from the values assumed on Γ by the singular solutions ψ^A and ψ^B introduced in Section 2.2. The Dirichlet condition is $\psi'_{|\Gamma} = -(\psi^A + \psi^B)_{|\Gamma}$. Taking into account the boundary values imposed on ψ^A by the conditions (2.4) and their counterpart for ψ^B, it is immediate to obtain the Dirichlet condition for ψ' on each of the four sides:

$$\begin{gathered} \psi'_{|\Gamma_t} = 0, \\ \psi'_{|\Gamma_l} = -\psi^B_{|\Gamma_l}, \quad \psi'_{|\Gamma_r} = -\psi^A{}_{|\Gamma_r}, \\ \psi'_{|\Gamma_b} = -(\psi^A + \psi^B)_{|\Gamma_b}. \end{gathered} \tag{3.4}$$

The Neumann condition for ψ' on each side is obtained by the same argument:

$$\begin{gathered} \frac{\partial \psi'}{\partial n}_{|\Gamma_t} = -1, \\ \frac{\partial \psi'}{\partial n}_{|\Gamma_l} = -\frac{\partial \psi^B}{\partial n}_{|\Gamma_l}, \quad \frac{\partial \psi'}{\partial n}_{|\Gamma_r} = -\frac{\partial \psi^A}{\partial n}_{|\Gamma_r}, \\ \frac{\partial \psi'}{\partial n}_{|\Gamma_b} = -\frac{\partial(\psi^A + \psi^B)}{\partial n}_{|\Gamma_b}. \end{gathered} \tag{3.5}$$

In terms of the Cartesian components of velocity, (u^A, v^A) and (u^B, v^B), these Neumann

conditions for ψ' read

$$\begin{gathered}\frac{\partial\psi'}{\partial n}_{|\Gamma_t} = -1,\\ \frac{\partial\psi'}{\partial n}_{|\Gamma_l} = -v^B_{|\Gamma_l}, \quad \frac{\partial\psi'}{\partial n}_{|\Gamma_r} = +v^A_{|\Gamma_r},\\ \frac{\partial\psi'}{\partial n}_{|\Gamma_b} = (u^A + u^B)_{|\Gamma_b}.\end{gathered} \tag{3.6}$$

Since the singular component ψ^{A+B} has accounted for the original incompatibility of the boundary data at the two corners without introducing any further incompatibility, the boundary conditions for the perturbation unknown ψ' satisfy all of the compatibility conditions for the biharmonic problem stated by Bernardi and Maday [4], as described in Section 2.1.

3.3. Time Discretization

For simplicity, the discretization in time of the vorticity equation is performed by means of a first-order-accurate time stepping, with an implicit account of the viscous term and a fully explicit treatment of the nonlinear Jacobian term. If the fields at $t = t_n$ are indicated by ω'_{old} and ψ'_{old}, while the unknowns at $t = t_{n+1}$ are indicated simply by ω' and ψ', the time discretized problem is

$$(-\nabla^2 + \gamma)\omega' = f \quad \text{and} \quad -\nabla^2\psi' = \omega', \tag{3.7}$$

where $\gamma = \mathrm{Re}/\Delta t$ and

$$f = \gamma\,\omega'_{\text{old}} + \nabla^2\omega^{A+B} - \mathrm{Re}\, J(\omega'_{\text{old}} + \omega^{A+B},\ \psi'_{\text{old}} + \psi^{A+B}). \tag{3.8}$$

The biharmonic problem above is solved after recasting it in the uncoupled form [16]

$$\begin{gathered}(-\nabla^2 + \gamma)\omega' = f, \qquad \int_\Omega \eta\omega' = \oint_{\partial\Omega}\left(\frac{\partial\eta}{\partial n}\,a' - \eta b'\right);\\ -\nabla^2\psi' = \omega', \qquad \psi'_{|\partial\Omega} = a'.\end{gathered} \tag{3.9}$$

In the integral conditions above, η represents any function harmonic in the computational domain Ω, while a' and b' denote, respectively, the Dirichlet and Neumann boundary data for ψ' appearing, respectively, in (3.4) and (3.6).

3.4. Spatial Approximation

The spatial discretization of the two elliptic equations in (3.7) is achieved by means of the Galerkin–Legendre method of Shen [17], with polynomials of the same degree N in the two spatial directions (see also [1]). The integral conditions are satisfied according to the spectral counterpart of the classical Glowinski–Pironneau method described in [1]. The nonlinear term is calculated by means of a numerical quadrature based on the standard Gauss–Legendre integration rule [1].

In the algorithm without singularity subtraction, an exact evaluation of the quadratic nonlinear term by numerical integration is obtained by a Gauss–Legendre formula with $\frac{3}{2}(N+1)$ quadrature points. The inclusion of the singular terms, which are not integrated exactly by the Gauss formula, entails aliasing errors. In order to appraise these errors, a

TABLE I
Convergence of $\omega(0, 0.95)$ for Different Degrees of the Basis and a Different Number of Quadrature Points (Re = 100)

N	$(N+1)$	$\frac{3}{2}(N+1)$	$2(N+1)$
16	−36.569	−36.194	−36.178
24	−35.973	−36.043	−36.045
32	−36.115	−36.088	−36.088
48	−36.082	−36.078	−36.078
64	−36.076	−36.077	−36.077
96	−36.076	−36.076	−36.076

comparison of the accuracy of the algorithm with a different number of quadrature points has been carried out, as reported in Table I. It can be seen that while a quite remarkable difference exists between results obtained with $N+1$ and $\frac{3}{2}(N+1)$ points for N low, increasing the number of quadrature points to $2(N+1)$ does not significantly improve the accuracy. This observation led us to retain the standard $\frac{3}{2}(N+1)$ Gauss–Legendre quadrature rule.

A better convergence rate might be achieved by analytically integrating the singular terms or by introducing *ad hoc* quadrature schemes for such terms. However, this would introduce an unwanted complication in the algorithm since the tensor product structure would be lost in the treatment of these terms.

A fundamental aspect in computing the right hand side (3.8) is the evaluation of the singular component $(\omega^{A+B}, \psi^{A+B})$ at the Gauss–Legendre points without transforming it in the basis function space, that is, without computing the expansion coefficients in the assumed polynomial basis. This consideration applies to both the term $\nabla^2\omega^{A+B}$ and the nonlinear term. The former is, however, the most critical one since it involves the second-order derivatives and has to be treated with particular care. After it is expressed in a weak variational form through an integration by parts, the resulting inner product $(\nabla w, \nabla\omega^{A+B})$, evaluated from the point values of $\nabla\omega^{A+B}$ by means of the Gauss–Legendre numerical quadrature, is necessarily inaccurate due to the singular behavior of ω^{A+B}.

In order to avoid explicit use of $\nabla^2\omega^{A+B}$ and of its weak substitutive equivalent, Eqs. (2.5) and (2.6) satisfied by the first and second terms of the singularity can be exploited. Noting that $\omega_0^{A+B} = \omega_0^A + \omega_0^B$ and $\omega_1^{A+B} = \omega_1^A + \omega_1^B$, Eqs. (2.5) and (2.6) imply, respectively,

$$\nabla^2\omega_0^{A+B} = 0, \tag{3.10}$$

$$\nabla^2\omega_1^{A+B} = J\big(\omega_0^A,\ \psi_0^A\big) + J\big(\omega_0^B,\ \psi_0^B\big). \tag{3.11}$$

As a consequence, the right hand side (3.8) is expressed in the form

$$\begin{aligned} f = \gamma\,\omega'_{\text{old}} - \text{Re}\big\{ & J\big(\omega'_{\text{old}} + \omega_1^{A+B},\ \psi'_{\text{old}} + \psi^{A+B}\big) \\ & + J\big(\omega_0^A, \psi'_{\text{old}} + \psi_0^B + \psi_1^{A+B}\big) + J\big(\omega_0^B, \psi'_{\text{old}} + \psi_0^A + \psi_1^{A+B}\big)\big\}, \end{aligned} \tag{3.12}$$

with the singular contributions appearing only in the "nonlinear" terms.

Since the evaluation of the terms of (3.12) is less critical—no second derivative is involved—a direct approach may be adopted: point values of the gradient $\nabla\psi^{A+B} = (-v^{A+B}, u^{A+B})$ are computed by means of the analytical expressions of the singular

solution given in [5], while point values of $\nabla\omega^{A+B}$ are computed according to the expressions which follow. Putting $\omega^A(r,\theta;\mathrm{Re}) = \omega_0^A(r,\theta) + \mathrm{Re}\,\omega_1^A(\theta)$, with $\omega_0^A(r,\theta) = \omega_0^A(\theta)/r$, the fields $\nabla\omega_0^A$ and $\nabla\omega_1^A$ of the Stokes and the first-order-in-Re contributions due to the singularity of corner A are

$$\begin{aligned} \alpha\,\frac{\partial\omega_0^A}{\partial x}(r,\theta) &= -\frac{1}{r^2}\,[2\sin(2\theta)+\pi\cos(2\theta)], \quad & \alpha^2\,\frac{\partial\omega_1^A}{\partial x}(r,\theta) &= -\frac{\sin\theta}{r}\,\Theta(\theta), \\ \alpha\,\frac{\partial\omega_0^A}{\partial y}(r,\theta) &= \frac{1}{r^2}\,[2\cos(2\theta)-\pi\sin(2\theta)], \quad & \alpha^2\,\frac{\partial\omega_1^A}{\partial y}(r,\theta) &= \frac{\cos\theta}{r}\,\Theta(\theta), \end{aligned} \tag{3.13}$$

where we have introduced the function

$$\Theta(\theta) = 4[-A_1 + (2B_1 - 3C_2 + 4B_2\theta)\cos(2\theta) + (2C_1 + 3B_2 + 4C_2\theta)\sin(2\theta)]. \tag{3.14}$$

For the expression of A_1, B_1, B_2, C_1, and C_2 the reader is referred to [5]. By symmetry considerations, the expressions for $\nabla\omega_0^B$ and $\nabla\omega_1^B$ of the two contributions due to the singularity of corner B are obtained in the form

$$\begin{aligned} \frac{\partial\omega_0^B}{\partial x}(r,\theta) &= -\frac{\partial\omega_0^A}{\partial x}(r,\pi-\theta), \quad & \frac{\partial\omega_1^B}{\partial x}(r,\theta) &= -\frac{\partial\omega_1^A}{\partial x}(r,\pi-\theta), \\ \frac{\partial\omega_0^B}{\partial y}(r,\theta) &= \frac{\partial\omega_0^A}{\partial y}(r,\pi-\theta), \quad & \frac{\partial\omega_1^B}{\partial y}(r,\theta) &= \frac{\partial\omega_1^A}{\partial y}(r,\pi-\theta). \end{aligned} \tag{3.15}$$

This treatment of the singular contributions allows to fully exploit the accuracy of the proposed method.

4. NUMERICAL SOLUTIONS AND COMPARISONS

In this section we compare some results obtained using the method described in [1], which has no treatment for the singularity, with the results provided by the present method in which the singular component of the flow is accounted for analytically and separately from the regular one. The main purpose is to demonstrate that a spectral method can provide accurate results for the singular driven cavity problem even employing the vorticity and stream function equations. Some "punctual" comparisons of the present solutions with benchmark values will be given without pretending, however, to offer new reference values. Accurate benchmark data are in fact already available in recent works of Barragy and Carey, who employed a p-type finite element method [2], and of Botella and Peyret, who employed a collocation–Chebyshev projection method [5]. Older but not less accurate benchmark results were given by Olson and Tuann [14].

We compare also the spectral results obtained by subtracting only the zeroth-order term with those obtained by subtracting the complete singularity comprising both the zeroth-order and first-order-in-Re contributions. The numerical solutions are presented mainly for the vorticity field, since it is the flow variable with the lowest regularity. Note that no filter has been applied, neither to obtain the displayed data nor to produce the plots.

First numerical comparisons for the steady flow are provided in Section 4.1; then solutions of the time-dependent singular driven cavity problem are presented in Section 4.2.

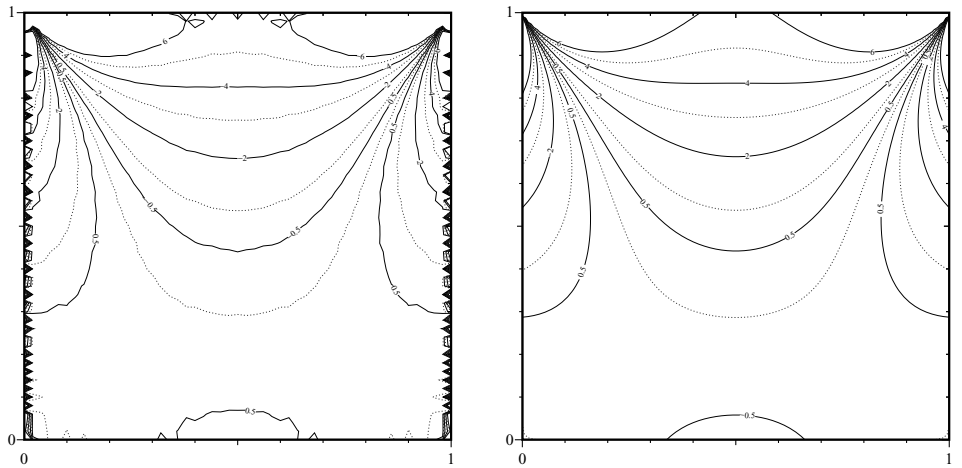

FIG. 4. Vorticity levels of the Stokes solution without (left) and with (right) subtraction of the corner singularity for $N = 50$.

4.1. Comparisons of Steady Solutions

Let us start by comparing the spectral solution provided by the original method [1] not containing any treatment for the singularity, with the solution obtained by the method that subtracts the singular components associated with the two upper corners. In Fig. 4 the two vorticity solutions for 50×50 polynomials are given. Strong Gibbs' oscillations are present in the solution of the first method, localized mainly on and near the vertical walls. By contrast the method with singularity subtraction yields a very smooth vorticity field everywhere in the cavity. The smoothness of the solutions obtained by the present spectral method is also illustrated by Fig. 5, which contains numerical solutions to the Stokes problem corresponding to 10^2 and 100^2 Legendre modes.

The accuracy of the ψ-ω spectral solution to the Stokes flow is verified by comparing the values of ψ at the local extrema in the primary and secondary vortices with the benchmark

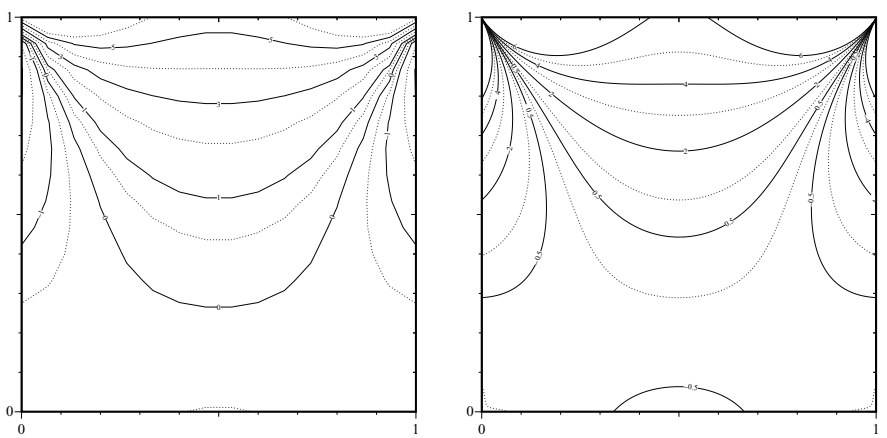

FIG. 5. Vorticity levels of the Stokes solution with subtraction of the corner singularity using $N = 10$ (left) and $N = 100$ (right).

TABLE II
Solution to the Stokes Problem

	N	$\boldsymbol{u}$-p [5]	ω-ψ present
ψ at primary vortex	12	0.10007 630	0.10007 62580
	16	0.10007 627	0.10007 62657
	24	0.10007 627	0.10007 62656
	48	0.10007 627	0.10007 62656
	96		0.10007 62656
ψ at secondary vortex	12	-2.1657×10^{-6}	$-2.12970\,684 \times 10^{-6}$
	16	-2.2255×10^{-6}	$-2.23269\,186 \times 10^{-6}$
	24	-2.2279×10^{-6}	$-2.22771\,733 \times 10^{-6}$
	48	-2.2276×10^{-6}	$-2.22757\,111 \times 10^{-6}$
	96		$-2.22757\,114 \times 10^{-6}$
ω(0, 0.95)	12	−27.27894	−27.27858 705
	16	−27.27898	−27.27896 477
	24	−27.27903	−27.27903 216
	48	−27.27901	−27.27900 888
	96		−27.27900 971

results provided by the spectral projection method of Botella and Peyret, reported in Table II. With the same number of modes, the values ψ of the present method and those computed from the $\boldsymbol{u}$-p solution are of a comparable accuracy. The solution with about 100 polynomials in each direction gives values with up to 10 exact significant digits. The values of vorticity in the point (0, 0.95), near to the top right corner, are also compared in Table II and the present spectral method is again found to be as accurate as the projection scheme.

We now consider nonzero Reynolds numbers. In Fig. 6, the steady spectral solution for $\mathrm{Re} = 100$ calculated with a spatial resolution of 30^2 modes without any singularity subtraction is compared with the two solutions obtained by subtracting only the Stokes singular component and by subtracting both the Stokes and the inertial singular components. These two latter vorticity fields compare well with the benchmark solution provided in [5], the complete singularity treatment producing a smoother solution. In the plottings, the improvement provided by including the inertial component in the singularity subtraction appears to be marginal with respect to the gain achieved by subtracting only the Stokes singular component. A more significant comparison is, however, possible by inspecting point values of the vorticity and comparing them to the benchmark values [5] given in Table III. Here we see that the subtraction of the full singularity leads to an appreciably faster convergence than the removal of only the Stokes component, especially near the singular corners.

In Fig. 7 the steady-state solutions for the higher value $\mathrm{Re} = 1000$ provided by the method with singularity treatment are compared for a spatial approximation using 100^2 degrees of freedom. Gibbs' oscillations affect the vorticity field computed without the singularity subtraction, without however destroying the qualitative meaning of the results. The solution provided by the singularity corrected method is remarkably much more accurate. The accuracy is assessed by comparing our results with the benchmark solution given in [5]. In Table IV the vorticity value at the point (0, 0.95) is reported for different values of N. The comparison with the reference results is excellent. The same conclusions can be drawn from Tables V and VI, where the vorticity point values on the horizontal and vertical centerlines are reported.

TABLE III
Solution for Re = 100

	N	$\boldsymbol{u}$-p [5]	ω-ψ present, full singularity	ω-ψ present$_0$, Stokes singularity
ω(0, 0.95)	24	−35.88211	−36.04297 509	−35.96656 957
	32	−36.13314	−36.08831 142	−36.08366 102
	48	−36.08094	−36.07841 854	−36.00327 582
	64	−36.07343	−36.07657 815	−35.99108 960
	96	−36.07535	−36.07621 984	−36.06454 716
ω(0.5, 0.5)	24	1.17437 5	1.17484 481	1.17510 994
	32	1.17441 0	1.17454 933	1.17460 211
	48	1.17441 2	1.17443 524	1.17443 577
	64	1.17441 2	1.17441 837	1.17441 625
	96	1.17441 2	1.17441 316	1.17441 213
ω(0.5, 1)	24	6.56746 3	6.56256 181	6.57120 043
	32	6.56478 4	6.56390 601	6.56680 472
	48	6.56416 1	6.56412 805	6.56496 515
	64	6.56410 7	6.56412 084	6.56448 320
	96	6.56409 1	6.56410 387	6.56420 977

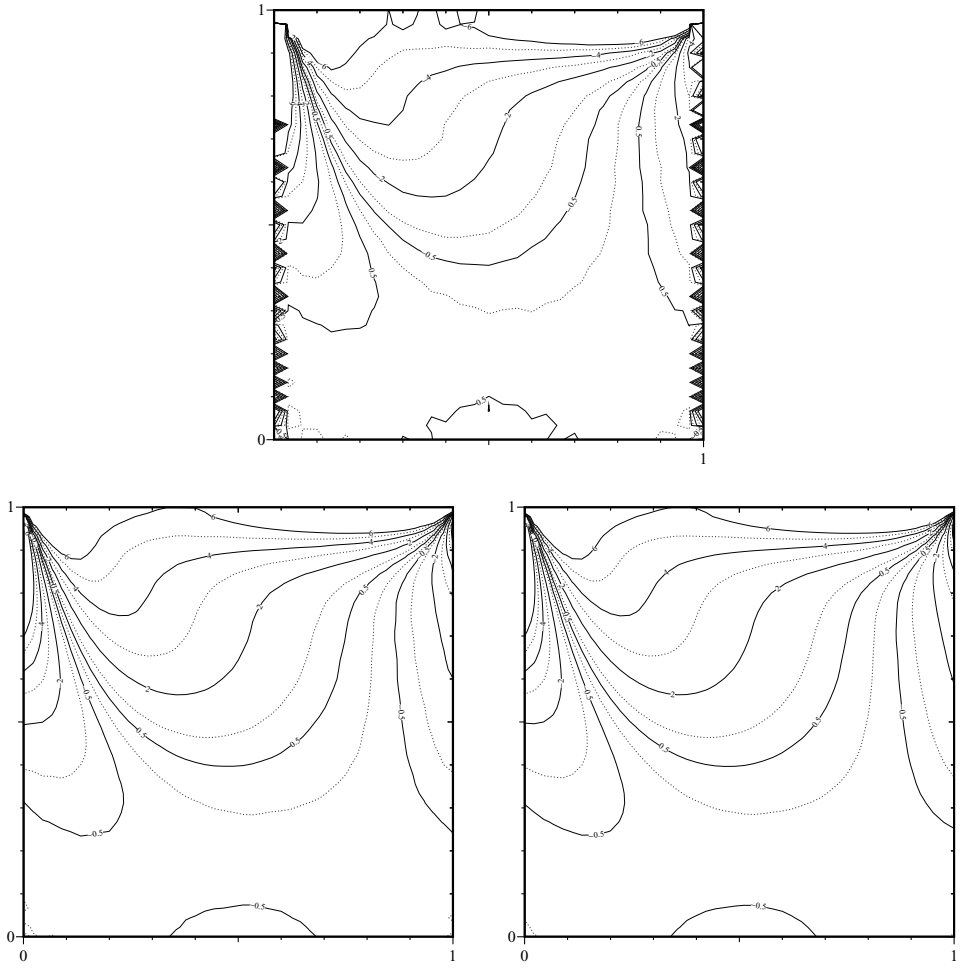

FIG. 6. Vorticity levels of the steady solutions for Re = 100 and $N = 30$ using the subtraction of the singular solution. (Top) No subtraction of the singularity; (bottom left) subtraction of only the zeroth-order contribution; (bottom right) subtraction of the complete singular solution.

TABLE IV
Solution for Re = 1000

	N	$\boldsymbol{u}$-p [5]	ω-ψ present, full singularity
ω(0, 0.95)	48	−84.24558	−83.99790
	64	−83.47874	−83.80990
	96	−83.70878	−83.80291
	128	−83.88577	−83.82139
	160	−83.82351	−83.82184

TABLE V
Solution for Re = 1000, ω(0.5, y)

y	32^2	64^2	128^2	160^2	160^2 [5]
0.0000	−4.16657	−4.16651	−4.16649	−4.16649	−4.16648
0.0547	−2.44035	−2.44934	−2.44963	−2.44959	−2.44960
0.0625	−2.31193	−2.31768	−2.31787	−2.31786	−2.31786
0.0703	−2.20460	−2.20221	−2.20173	−2.20176	−2.20175
0.1016	−1.62867	−1.63462	−1.63436	−1.63437	−1.63436
0.1719	1.06128	1.05470	1.05464	1.05467	1.05467
0.2813	2.26942	2.26730	2.26774	2.26771	2.26772
0.4531	2.07067	2.06238	2.06216	2.06215	2.06215
0.5000	2.05827	2.06751	2.06724	2.06722	2.06722
0.6172	2.06797	2.06496	2.06543	2.06540	2.06539
0.7344	2.09625	2.09145	2.09124	2.09120	2.09121
0.8516	1.76898	1.76220	1.76204	1.76201	1.76200
0.9531	4.44763	4.86093	4.85743	4.85757	4.85754
0.9609	6.51359	6.95836	6.95974	6.95970	6.95968
0.9688	9.36122	9.48878	9.49513	9.49496	9.49496
0.9766	12.60600	12.06556	12.06722	12.06693	12.0670
1.0000	14.32910	14.75547	14.75381	14.75361	14.7534

TABLE VI
Solution for Re = 1000, ω(x, 0.5)

x	32^2	64^2	128^2	160^2	160^2 [5]
0.0000	−5.59602	−5.47227	−5.46258	−5.46226	−5.46217
0.0312	−8.41640	−8.44494	−8.44340	−8.44349	−8.44350
0.0391	−8.22466	−8.24544	−8.24611	−8.24614	−8.24616
0.0469	−7.58278	−7.58509	−7.58528	−7.58522	−7.58524
0.0547	−6.51158	−6.50946	−6.50871	−6.50866	−6.50867
0.0937	0.91697	0.92320	0.92287	0.92290	0.92291
0.1406	3.42823	3.43005	3.43013	3.43015	3.43016
0.1953	2.21912	2.21172	2.21169	2.21172	2.21171
0.5000	2.05827	2.06751	2.06724	2.06722	2.06722
0.7656	2.05351	2.06169	2.06119	2.06121	2.06122
0.7734	1.98639	2.00231	2.00177	2.00175	2.00174
0.8437	0.73193	0.74280	0.74204	0.74206	0.74207
0.9062	−0.79667	−0.82320	−0.82403	−0.82399	−0.82398
0.9219	−1.25534	−1.24106	−1.23994	−1.23990	−1.23991
0.9297	−1.49816	−1.50299	−1.50306	−1.50308	−1.50306
0.9375	−1.77974	−1.83182	−1.83303	−1.83309	−1.83308
1.0000	−7.60270	−7.66347	−7.66389	−7.66385	−7.66369

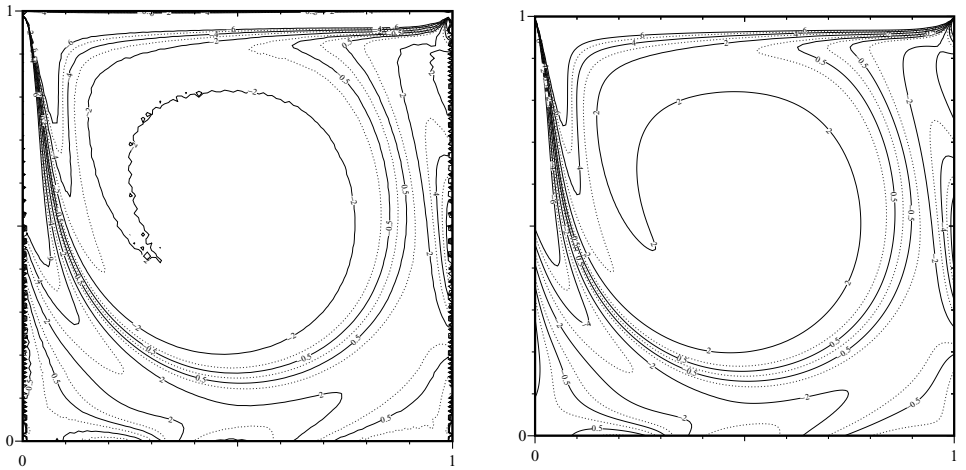

FIG. 7. Vorticity levels of the steady solutions for $\mathrm{Re} = 1000$ and $N = 100$. Comparison of spectral solutions without singularity treatment (left) and with subtraction of the singular solution (right).

4.2. Comparisons of Unsteady Solutions

Let us consider the evolutionary problem of the driven cavity with an impulsive start of the wall and the fluid initially at rest in the whole domain. The initial condition for the perturbation problem is readily deduced from the condition of zero vorticity, $\omega(\boldsymbol{x}, 0) = 0$, recast for the vorticity perturbation unknown $\omega' = \omega - \omega^{A+B}$, to give

$$\omega'(\boldsymbol{x}, 0) = -\omega^{A+B}(\boldsymbol{x}).$$

Thus the first time step is computed with $\omega'_{\mathrm{old}} = -\omega^{A+B}(\boldsymbol{x})$, evaluated in weak form by a L^2 projection performed numerically, relying upon Gauss–Legendre quadrature points;

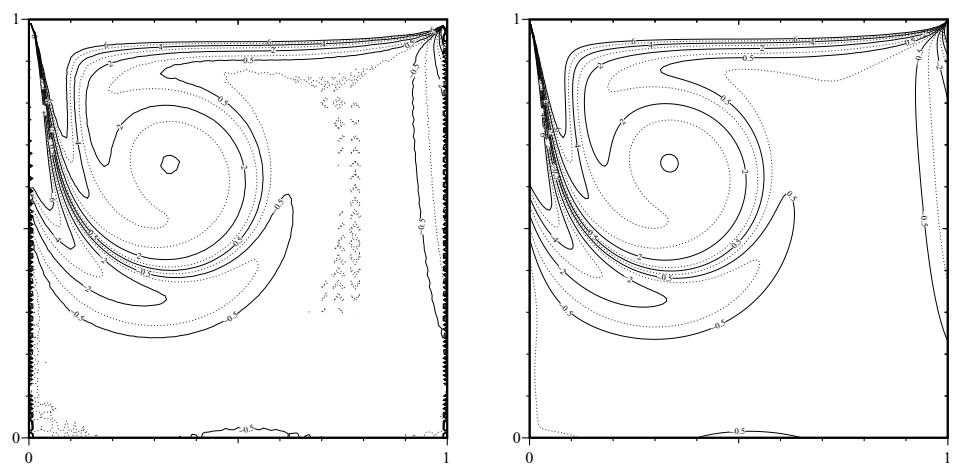

FIG. 8. Instantaneous vorticity field for the impulsively started driven cavity problem at $t = 6.25$ for $\mathrm{Re} = 1000$ and with $N = 100$. (Left) No treatment for the corner singularity; (right) subtraction of the solution singular component.

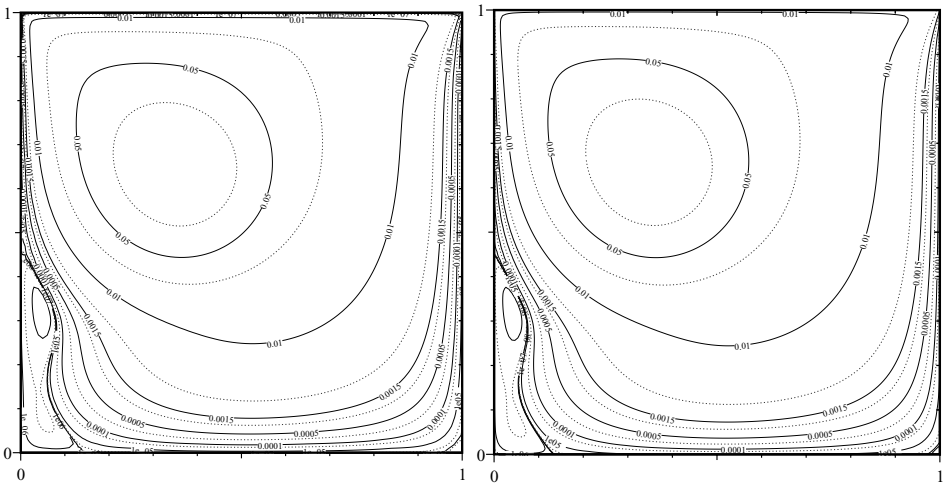

FIG. 9. Instantaneous streamlines for the impulsively started driven cavity problem at $t = 6.25$ for $\mathrm{Re} = 1000$ and with $N = 100$. (Left) No treatment for the corner singularity; (right) subtraction of the solution singular component.

the nonlinear term of (3.3) is initially zero, and Eq. (3.12) for $t = 0$ reduces to $f_{|t=0} = -\gamma\omega^{A+B} + \mathrm{Re}J(\omega_0^A, \psi_0^A) + \mathrm{Re}J(\omega_0^B, \psi_0^B)$.

The adequacy of the subtraction technique also for computing time-dependent solutions has been assessed considering $\mathrm{Re} = 1000$. In Figs. 8 and 9 we compare, respectively, the vorticity field and the streamlines of two spectral solutions with 100^2 degrees of freedom, at time $t = 6.25$. The solution on the left is obtained with no singularity treatment, while the solution on the right is provided by the spectral method with subtraction of the corner singularity. The vorticity field of the first method is polluted by Gibbs' phenomenon, with strong oscillations localized near the vertical walls. It must be noted that, irrespective of these appreciable spatial oscillations, the vorticity field in the interior of the cavity is almost indistinguishable from that obtained by a FEM formulation solving the equations for the stream function and the vorticity with a fully explicit treatment of the viscous term in the dynamical equation [8]. The vorticity levels of the spectral method with a proper handling of the corner singularity are smooth. The comparison between the streamlines provided by the two methods shown in Fig. 9 confirms that the Gibbs' polluted spectral solution still reproduces the dynamics of detailed features of the flow, in this case the coalescence of two vortices along the downstream vertical wall to form a single secondary eddy in the downstream bottom corner of the cavity at later stages of the transient.

5. CONCLUSIONS

A spectral technique for the accurate solution of the singular driven cavity problem in the vorticity and stream function representation has been proposed. The method implements the singularity subtraction technique proposed by Botella and Peyret [5] for the primitive variable projection method and is based on the Galerkin–Legendre spectral solver for the vorticity and stream function equations presented in [1]. The equations are solved in an uncoupled manner by imposing vorticity integral conditions by means of the spectral counterpart of the Glowinski–Pironneau method implemented in [1].

The numerical results presented in the paper demonstrate that the singular problem can be solved accurately, even using the nonprimitive variables, without smoothing the boundary conditions in the singular corners. As in [5], both the Stokes and the first-order-in-Re components of the singular solution have been considered. The inclusion of these two components is found to guarantee greater accuracy than when including only the Stokes singular component in the considered Reynolds number interval ($\mathrm{Re} \leq 1000$).

In developing the algorithm, the evaluation of the various terms involving the singular component of the solution has required a very careful treatment. For instance, it has been found that a straightforward handling of the linear and nonlinear explicit terms in the vorticity equation can lead to a degradation of the accuracy of the method. In particular, the singular components of vorticity and stream function must be retained in the physical space, while the regular component is handled in the space of the Legendre coefficients. In this connection, it can be noted that the accuracy of the singularity subtraction technique might be enhanced by resorting to a conformal mapping of the local coordinates of each singular region of the problem, as recently proposed by Pathria and Karniadakis for Laplace, Poisson, and Helmholtz equations [15]. The viability of this approach to the Stokes operator in the presence of nonlinear terms and under more than one singularity is certainly a matter worthy of investigation.

The most distinctive characteristic of the proposed method lies in the adoption of a modal, hierarchical basis instead of the classical Lagrangian basis. This basis allows complete freedom in the choice of the numerical integration rule, which is not the case of collocation-oriented bases, implying necessarily the use of a Gauss–Lobatto quadrature formula to enforce Dirichlet boundary conditions. As a consequence, the classical Gauss–Legendre quadrature formula is here employed, which does not require a sampling of the singularity in the upper corners, in contrast to the Gauss–Lobatto formula. To accurately evaluate the integrals involving the singular component(s) of the solution it is sufficient to adopt the standard $\frac{3}{2}(N+1)$ rule, also needed for the exact computation of the quadratic nonlinear terms.

The results obtained for steady solutions are found to be in a perfect agreement with, and also more accurate than, the benchmark spectral results of [5]. Moreover, the singularity subtraction technique adopted here, although based on singular solutions of the steady problem, is found to be adequate for obtaining accurate spectral solutions also for the unsteady version of the singular driven cavity problem.

REFERENCES

1. F. Auteri and L. Quartapelle, Galerkin spectral method for the vorticity and stream function equations, *J. Comput. Phys.* **141**, 306 (1999).
2. E. Barragy and G. F. Carey, Stream function–vorticity driven cavity solution using p finite elements, *Comput. Fluids* **26**, 455 (1997).
3. G. F. Batchelor, *An Introduction to Fluid Dynamics* (Cambridge Univ. Press, Cambridge, 1967).
4. C. Bernardi and Y. Maday, *Approximations Spectrales des Problèmes aux Limites Elliptiques* (Springer-Verlag, Paris, 1992).
5. O. Botella and R. Peyret, Benchmark spectral results on the lid-driven cavity flow, *Comput. Fluids* **27**, 421 (1998).
6. O. R. Burggraf, Analytical and numerical studies of the structure of steady separated flow, *J. Fluid Mech.* **24**, 113 (1966).
7. U. Ghia, N. Ghia, and C. T. Shin, High-Re solutions for incompressible flow using the Navier–Stokes equations and a multigrid method, *J. Comput. Phys.* **48**, 387 (1982).

8. J.-L. Guermond and L. Quartapelle, Weak formulation of the ψ-ω equations with explicit viscous diffusion, *Mathematical Models and Methods in Applied Sciences* **10**, 85 (2000).
9. M. M. Gupta, R. P. Manohar, and B. Noble, Nature of viscous flows near sharp corners, *Comput. Fluids* **9**, 379 (1981).
10. C. Hancock, E. Lewis, and H. K. Moffatt, Effects of inertia in forced corner flows, *J. Fluid Mech.* **112**, 315 (1981).
11. D. B. Ingham and M. A. Kelmanson, *Boundary Integral Equation Analyses of Singular, Potential, and Biharmonic Problems*, Lecture Notes in Engineering (Springer-Verlag, Berlin, 1984), Vol. 7.
12. M. A. Kelmanson, Modified integral equation solution of viscous flows near sharp corners, *Comput. Fluids* **11**, 307 (1983).
13. J. Koplik and J. R. Banavar, Corner flow in the sliding plate problem, *Phys. Fluids* **7**, 3118 (1995).
14. M. D. Olson and S.-Y. Tuann, New finite element results for the square cavity, *Comput. Fluids* **7**, 123 (1979).
15. D. Pathria and G. E. Karniadakis, Spectral element methods for elliptic problems in nonsmooth domains, *J. Comput. Phys.* **122**, 83 (1995).
16. L. Quartapelle, *Numerical Solution of the Incompressible Navier–Stokes Equations* (Birkhäuser, Basel, 1993).
17. J. Shen, Efficient spectral–Galerkin method. I. Direct solvers of second- and fourth-order equations using Legendre polynomials, *SIAM J. Sci. Comput.* **15**, 1489 (1994).
18. W. W. Schultz, N. Y. Lee, and J. P. Boyd, Efficient spectral–Galerkin method. I. Direct solvers of second- and fourth-order equations using Legendre polynomials, *SIAM J. Sci. Comput.* **15**, 1489 (1994).